

## Structural, electronic, and magnetic properties of small rhodium clusters

Yang Jinlong

*International Center for Materials Physics, Academia Sinica, Shenyang 110015, People's Republic of China  
and Center for Fundamental Physics, University of Science and Technology of China, Hefei, Anhui 230026,  
People's Republic of China\**

F. Toigo

*Dipartimento di Fisica dell'Università and Consorzio Interuniversitario di Struttura della Materia  
Istituto Nazionale Fisica della Materia, Via Marzolo 8, 35100 Padova, Italy*

Wang Kelin

*Center for Fundamental Physics, University of Science and Technology of China, Hefei, Anhui 230026,  
People's Republic of China*

(Received 14 February 1994; revised manuscript received 23 March 1994)

The structural, electronic, and magnetic properties of small  $\text{Rh}_N$  clusters ( $N = 2-8, 10, 12, 13$ , and 19) are studied using the discrete-variational local-spin-density-functional method. The ground-state structures of  $\text{Rh}_2$ ,  $\text{Rh}_3$ , and  $\text{Rh}_4$  are obtained and found to exhibit a tendency toward higher-dimensional geometries with longer bond lengths and more nearest-neighbor bonds. The equilibrium bond lengths in the chosen geometry for the  $\text{Rh}_5$ - $\text{Rh}_8$ ,  $\text{Rh}_{10}$ ,  $\text{Rh}_{12}$ , and  $\text{Rh}_{13}$  clusters are determined and show 4-6% bond length contractions compared with the bulk interatomic spacing. A complex size dependence of the magnetic properties of the  $\text{Rh}_N$  clusters is found to be consistent with a recent experiment. The average magnetic moment per atom of the  $\text{Rh}_N$  clusters varies from  $0\mu_B$  to  $2\mu_B$ . The clusters with magnetic ground states have ferromagnetic interactions, while the local moments of the  $5s$  and  $5p$  often align antiferromagnetically with that of the  $4d$ . The calculated magnetic moments of the  $\text{Rh}_{10}$ ,  $\text{Rh}_{12}$ ,  $\text{Rh}_{13}$ , and  $\text{Rh}_{19}$  clusters are compared and discussed with the experimental ones. Icosahedral growth is suggested for Rh clusters. The reactivity of the  $\text{Rh}_N$  clusters toward  $\text{H}_2$ ,  $\text{N}_2$ , and  $\text{CO}$  molecules is predicted. The densities of states, exchange splittings, valence band widths, and ground-state electronic configurations are presented for all the clusters. Finally an energy difference is identified which may be used as the criterion for the existence of multiple magnetic solutions in local-spin-density-functional calculations.

### I. INTRODUCTION

Small clusters have been a subject of intense investigation in recent years.<sup>1</sup> With quite large surface-to-volume ratio, a cluster may have electronic, optical, magnetic, and structural properties different from those of its bulk phase. Exploring these uncommon properties is of great importance in developing new cluster-based materials for technological applications. In addition, clusters may serve as models for understanding localized effects in solids.

Transition-metal (TM) clusters are of significant interest, due to their promising practical applications in developing new magnetic materials with large moments and new catalysts with high reactivity.<sup>2,3</sup> Many theoretical calculations<sup>4-17</sup> and experimental measurements<sup>18-22</sup> have been done for  $3d$  TM clusters. Both theoretical and experimental studies<sup>4-9,19,20,22</sup> of small Fe, Co, and Ni clusters have indicated that cluster atoms have larger average magnetic moment per atom than atoms in the bulk phase, and found that the average moment per atom in these clusters is almost independent of the cluster size.

Theoretical calculations<sup>7,11</sup> also predicted nonzero magnetic moments for other  $3d$  TM clusters, though their corresponding bulk phases have no moments. Such an expectation is reasonable because of the reduced coordination and of the high symmetry of clusters. These attributes narrow the  $d$ -band widths and offer the possibility of large spin multiplicities in the electronic ground states. Unfortunately, experimental measurements<sup>18,21</sup> have so far given nonmagnetic results in the experimental resolution limits.

For  $4d$  TM clusters, there are only a few studies from theory and experiment. Using the local-spin-density-functional (LSD) theory, Reddy *et al.*<sup>23</sup> proposed that 13-atom clusters of Pd, Rh, and Ru will be magnetic. Indeed, Cox *et al.*<sup>24</sup> observed experimentally giant magnetic moments in small  $\text{Rh}_N$  clusters with  $N = 9-34$ , while their observed value of the average moment per atom for  $\text{Rh}_{13}$  is  $0.48\mu_B$ , only about one-third of the  $1.62\mu_B$  predicted by Reddy *et al.* They also observed that the average moment per atom of the Rh clusters depends significantly on cluster size. There are several special sizes,  $\text{Rh}_{15}$ ,  $\text{Rh}_{16}$ , and  $\text{Rh}_{19}$ , that are unusually

magnetic relative to adjacent clusters. There are also a few clusters that appear to be relatively nonmagnetic. Recently, we<sup>25</sup> have performed a first-principles study on the electronic structures of Rh<sub>13</sub> clusters with three possible high-symmetry geometries. We found an anomalous relationship between the cluster symmetry and the magnetism of Rh<sub>13</sub> clusters, i.e., the total moment of the icosahedral Rh<sub>13</sub> cluster is smaller than that of the lower-symmetry clusters in a wide range of interatomic spacings.

In this paper, we perform a comprehensive first-principles study of Rh<sub>N</sub> clusters with  $N = 2-8, 10, 12, 13,$  and  $19$  in the hope of understanding the size dependence of the structural, electronic, and magnetic properties of small rhodium clusters. The ground-state structures of Rh<sub>2</sub>, Rh<sub>3</sub>, and Rh<sub>4</sub> clusters are determined by maximizing the calculated binding energies for the possible geometries. Since the number of possible geometries increases quite rapidly with cluster size, it becomes impossible to determine the ground-state structures of the larger clusters with this method. We assume one probable geometry for each of the larger clusters and optimize its bond lengths. The geometries we chose for the clusters are shown in Fig. 1. We describe our theoretical method in Sec. II and present our results and discussions in Sec. III. Finally a summary is given in Sec. IV.

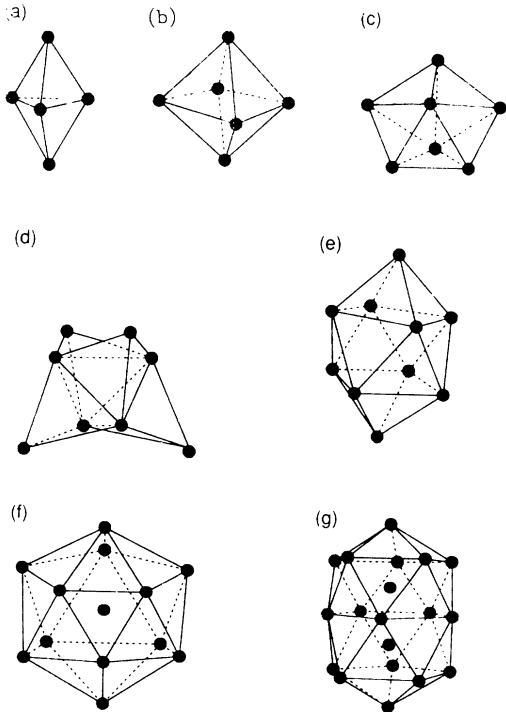


FIG. 1. Geometries of clusters. (a)  $N = 5$ , trigonal bipyramid ( $D_{3h}$ ), (b)  $N = 6$ , octahedron ( $O_h$ ), (c)  $N = 7$ , pentagonal bipyramid ( $D_{5h}$ ), (d)  $N = 8$ , tetrahedral multitwin ( $T_d$ ), (e)  $N = 10$ , twisted double square pyramid ( $D_{4d}$ ), (f)  $N = 12$  and  $13$ , icosahedron ( $I_h$ ), and (g)  $N = 19$ , double icosahedron ( $D_{5h}$ ).

## II. METHOD

The binding energy and electronic structure of clusters are calculated using the discrete-variational (DV) LSD method. It is a kind of molecular orbital calculation method, and its theoretical foundation is LSD theory. Since it has been described in detail elsewhere,<sup>26,27</sup> here we only summarize its main points and discuss the choice of computational parameters.

(a) The one-electron equation underlying the DV-LSD method is

$$(h_\sigma - \varepsilon_{i\sigma})\psi_{i\sigma} = (-\frac{1}{2}\nabla^2 + v_c + v_{xc}^\sigma - \varepsilon_{i\sigma})\psi_{i\sigma} = 0, \quad (1)$$

where the one-electron Hamiltonian includes the electron-nucleus and electron-electron Coulomb potential  $v_c$  and the spin-dependent exchange-correlation potential  $v_{xc}^\sigma$ . This last is a function of the electron density for each spin  $\sigma$ ,  $\rho_\sigma(\mathbf{r})$ , given by

$$\rho_\sigma(\mathbf{r}) = \sum_i n_{i\sigma} |\psi_{i\sigma}(\mathbf{r})|^2, \quad (2)$$

where  $n_{i\sigma}$  is the occupation of the cluster spin orbital  $\psi_{i\sigma}$ , chosen according to Fermi-Dirac statistics. In our calculations, we take  $v_{xc}^\sigma$  to be of the von Barth-Hedin form,<sup>28</sup> with the parameters taken from Moruzzi *et al.*<sup>29</sup> We also used the Perdew-Zunger form<sup>30</sup> for a few cases and found that the calculated results are independent of the form of  $v_{xc}^\sigma$ .

(b) The cluster spin orbitals are expanded in a linear combination of  $\chi_j(\mathbf{r})$ :

$$\psi_{i\sigma}(\mathbf{r}) = \sum_j \chi_j(\mathbf{r})c_{ji}^\sigma, \quad (3)$$

where the  $\chi_j(\mathbf{r})$  are the numerical symmetrized atomic basis functions that transform as one of the irreducible representations of the point group of the cluster. The numerical atomic basis functions are obtained from the self-consistent atomic local-density-functional (LDF) calculation. In our calculations, we choose the Rh  $4s^2 4p^6 4d^8 5s^{0.9} 5p^{0.1}$  configuration for the atomic basis functions to represent the valence electron orbitals. The rest of the core orbitals are frozen. Similar choices for other TM elements have been made,<sup>11,13,16,27</sup> where the calculated results compare well with those of other theoretical studies, obtained using higher-quality basis sets, and with the experimental ones.

(c) The one-electron equation (1) is approximately solved by the Rayleigh-Ritz variational method, which is done by using the expansion of  $\psi_{i\sigma}$  in Eq. (3) and minimizing certain error functions  $\Delta_{ij}^\sigma$  defined as

$$\Delta_{ij}^\sigma = \langle \psi_{i\sigma} | h_\sigma - \varepsilon | \psi_{j\sigma} \rangle. \quad (4)$$

This procedure leads to the secular equation

$$(\mathbf{H}^\sigma - \varepsilon \mathbf{S})\mathbf{C}^\sigma = 0. \quad (5)$$

(d) In the DV scheme, the matrix elements of the Hamiltonian matrix  $\mathbf{H}^\sigma$  and the overlap matrix  $\mathbf{S}$  are obtained by a weighted summation over a set of sample

points  $\mathbf{r}_k$  (diophantine points), i.e.,

$$H_{ij}^\sigma = \langle \chi_i | h_\sigma | \chi_j \rangle = \sum_k \omega(\mathbf{r}_k) \chi_i^*(\mathbf{r}_k) h_\sigma(\mathbf{r}_k) \chi_j(\mathbf{r}_k), \quad (6)$$

$$S_{ij} = \langle \chi_i | \chi_j \rangle = \sum_k \omega(\mathbf{r}_k) \chi_i^*(\mathbf{r}_k) \chi_j(\mathbf{r}_k), \quad (7)$$

where the  $\omega(\mathbf{r}_k)$ 's are appropriate integration weights. In our numerical integrations, about 4000 sampling points per atom for the clusters with  $N \leq 4$  and 2000 for the others are adopted. With these points, we found sufficient convergence for both the electronic spectrum and the binding energy.

(e) To facilitate the computational procedure for building the cluster potential, a multipolar, multicenter model density is used to fit the exact cluster charge density with a least-squares error-minimization procedure:

$$\varrho(\mathbf{r}) \simeq \varrho_M(\mathbf{r}) = \sum_{i,l,m} \varrho_{lm}^i(r_i) Y_{lm}(\hat{\mathbf{r}}_i), \quad (8)$$

where  $i$  denotes multipoles centered on various nuclear sites at  $\mathbf{r}_i$ , and  $\varrho(\mathbf{r})$  is the total electron density  $\varrho_\uparrow + \varrho_\downarrow$ . An equivalent expansion is made for the spin density  $\varrho_\uparrow - \varrho_\downarrow$ . We obtained good fitting accuracy for the charge density of the  $\text{Rh}_N$  clusters by including multipoles up to  $l = 2$  in Eq. (8).

(f) The total energy of a cluster in the LSD approximation is written in standard notation as

$$\begin{aligned} E_{\text{tot}} &= \sum_{i\sigma} n_{i\sigma} \varepsilon_{i\sigma} - \frac{1}{2} \int \int \frac{\varrho(\mathbf{r})\varrho(\mathbf{r}')}{|\mathbf{r} - \mathbf{r}'|} d\mathbf{r} d\mathbf{r}' \\ &+ \sum_\sigma \int \varrho_\sigma(\mathbf{r}) [\varepsilon_{\text{xc}}(\mathbf{r}) - v_{\text{xc}}^\sigma(\mathbf{r})] d\mathbf{r} \\ &+ \frac{1}{2} \sum_\mu \sum_\nu' \frac{Z_\mu Z_\nu}{R_{\mu\nu}} \\ &\equiv \int e(\mathbf{r}) d\mathbf{r} + \frac{1}{2} \sum_\mu \sum_\nu' \frac{Z_\mu Z_\nu}{R_{\mu\nu}}, \end{aligned} \quad (9)$$

where  $\varepsilon_{\text{xc}}$  is the exchange-correlation energy density, and  $e(\mathbf{r})$  is an energy density. The binding energy of the cluster is then defined with respect to some reference system, say the dissociated atoms, as

$$E_b = -(E_{\text{tot}} - E_{\text{tot}}^{\text{ref}}), \quad (10)$$

where

$$E_{\text{tot}}^{\text{ref}} = \int e^{\text{ref}}(\mathbf{r}) d\mathbf{r}. \quad (11)$$

In the DV scheme, the numerical error of  $E_b$  is minimized with the point-by-point error-cancellation technique. In this technique, the reference system energy is computed with the same sampling grid as in the self-consistent-field and the cluster energy procedures by freezing the atoms at their respective lattice sites, but they are now assumed to be noninteracting, so that the numerical error of  $E_b$

can be partly canceled out via point-by-point subtraction of  $e(\mathbf{r}_k)$  and  $e^{\text{ref}}(\mathbf{r}_k)$ :

$$E_b = - \sum_k \omega(\mathbf{r}_k) [e(\mathbf{r}_k) - e^{\text{ref}}(\mathbf{r}_k)] - \frac{1}{2} \sum_\mu \sum_\nu' \frac{Z_\mu Z_\nu}{R_{\mu\nu}}. \quad (12)$$

### III. RESULTS AND DISCUSSIONS

The calculated binding energy for the  $\text{Rh}_2$  dimer is shown in Fig. 2 as a function of dimer separation for paramagnetic (PM) and ferromagnetic (FM) states. The resulting equilibrium bond length  $r_e$ , vibrational frequency  $\omega_e$ , and dissociation energy  $D_e$  are listed in Table I. The ground state is FM, with magnetic moment  $2\mu_B$  per atom. The FM state is more stable by 0.93 eV with a bond length larger by 0.06 Å than the PM state. The obtained dissociation energy for the FM state is 3.04 eV, in good agreement with the experimental one (2.92 eV).<sup>31</sup> Shim<sup>32</sup> had performed a configuration interaction calculation for the  $\text{Rh}_2$  dimer. His results are also listed in Table I. Compared with our results and with the experimental data, his  $r_e$ ,  $\omega_e$ , and  $D_e$  are undoubtedly far too long (in fact, longer than the bulk interatomic spacing), far too floppy, and far too weak respectively. As Salahub commented,<sup>33</sup> this is mainly due to the lack of an adequate correlation treatment in his calculation. In addition, we have not found any antiferromagnetic (AFM) solution for the  $\text{Rh}_2$  dimer by removing the symmetry constraints imposed on our calculations.

We have considered both the linear and trigonal geometries for the  $\text{Rh}_3$  trimer, and the resulting binding energies are shown in Fig. 3. It is obvious that the two-dimensional trigonal geometry is more stable than the one-dimensional linear chain. For both geometries, the cluster magnetic moments are sensitive to the bond length  $r$  and increase with increase of  $r$ . At the equilibrium configuration, the total moment of the trigonal  $\text{Rh}_3$  trimer is  $3\mu_B$ , larger than that of the linear chain, which

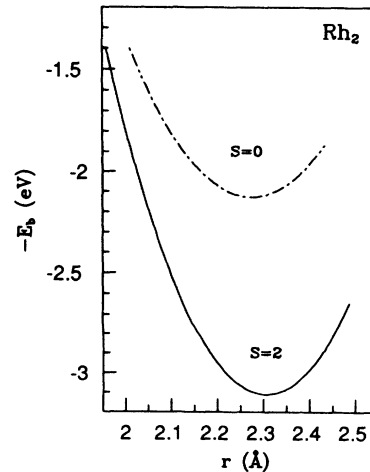


FIG. 2. Binding energy as a function of bond length for the  $\text{Rh}_2$  dimer.

TABLE I. Equilibrium bond length  $r_e$ , vibrational frequency  $\omega_e$ , and dissociation energy  $D_e$  for the  $\text{Rh}_2$  dimer.

	$r_e$ (Å)	$\omega_e$ ( $\text{cm}^{-1}$ )	$D_e$ (eV)
PM	2.25	292	2.11
FM	2.31	333	3.04
Shim (Ref. 32)	2.86	118	0.85
Expt. (Ref. 31)			2.92

is  $1\mu_B$ . The lowest-energy state of  $\text{Rh}_3$  is found to correspond to the isosceles triangle, which has slightly lower energy than the one in the equilateral triangle (Table II). The equilibrium bond lengths are 2.46, 2.46, and 2.34 Å, respectively. The corresponding bond angle is  $56.8^\circ$ .

The binding energy curves versus  $r$  for the  $\text{Rh}_4$  tetramer are plotted in Fig. 4. From this figure, one can see again that the cluster favors higher-dimensional geometry with longer bond lengths and more nearest-neighbor bonds. For the one- and two-dimensional geometries, we find that the magnetic state ( $S \neq 0$ ) has lower energy than the PM state. For the three-dimensional geometry, however, the situation is different. There is only one PM solution in a wide range of  $r$ , and the magnetic solution appears when  $r > 2.55$  Å. The energy curve for this magnetic solution has no stable minimal point. As a result, the ground state of  $\text{Rh}_4$  is PM. From Table II, it is interesting to note that the planar rhombus geometry has lower energy than the square geometry, while the trigonal pyramid has higher energy than the tetrahedral geometry.

The equilibrium properties for the  $\text{Rh}_5$ – $\text{Rh}_8$ ,  $\text{Rh}_{10}$ ,  $\text{Rh}_{12}$ ,  $\text{Rh}_{13}$ , and  $\text{Rh}_{19}$  clusters are presented in Table III. From the table, one may see that all clusters except  $\text{Rh}_6$  have magnetic ground states. The ground state of the  $\text{Rh}_6$  cluster is PM, the same as what we get for the  $\text{Rh}_4$  cluster. In contrast to the  $\text{Rh}_4$  cluster, however, the  $\text{Rh}_6$  cluster always has a higher-energy magnetic solution in addition to the PM solution, as shown in Fig. 5, and the energy curve for the magnetic solution has a stable minimal point. The  $\text{Rh}_8$ ,  $\text{Rh}_{10}$ , and  $\text{Rh}_{12}$  clusters also have both PM and magnetic equilibrium configurations, but now the magnetic states have lower energies

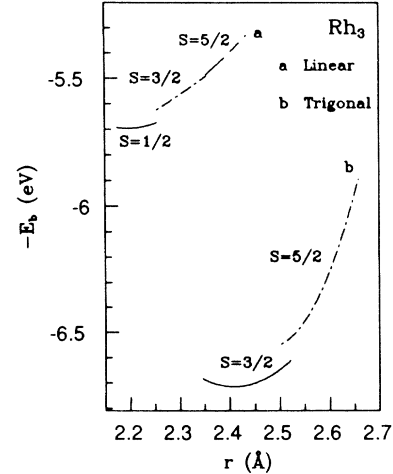


FIG. 3. Binding energy as a function of bond length for the  $\text{Rh}_3$  trimer.

and correspond to the ground states. For clusters with  $N \geq 10$ , moreover, we find that there is more than one self-consistent magnetic solution at the magnetic equilibrium configuration (Table III). We choose the one which gives the largest cluster binding energy as the actual magnetic solution for a cluster. We will further discuss the multiple solutions in terms of an energy parameter later.

For all clusters, once there exist both PM and magnetic equilibrium configurations for one geometry, we always obtain a longer equilibrium bond length for the magnetic state. This observation can be understood by noticing that the magnetic interaction leads to a splitting of the  $d$  bands and a filling of the less bonding majority-spin orbitals at the expense of the more bonding minority-spin orbitals.

Comparing to the bulk interatomic spacing of 2.69 Å, one may find there are bond-length contractions in all the  $\text{Rh}_N$  clusters. The value of the contraction varies from about 14% for the dimer, to 4–8% for the larger clusters. Such bond-length contractions have changed dramatically the magnetic properties of some clusters.

TABLE II. The equilibrium bond lengths and binding energies for the  $\text{Rh}_3$  and  $\text{Rh}_4$  clusters.

	Geometry	Symmetry	Spin	$r_e$ (Å)	$E_b$ (eV)
$\text{Rh}_3$	Linear chain	$D_{\infty h}$	$S = 1/2$	2.20	5.74
	Equilateral triangle	$C_{3v}$	$S = 3/2$	2.42	6.76
	Isosceles triangle	$C_{2v}$	$S = 3/2$	2.46, 2.34	6.78
$\text{Rh}_4$	Linear chain	$D_{\infty h}$	$S = 0$	2.19	7.98
			$S = 1$	2.22	8.22
	Square	$D_{4h}$	$S = 0$	2.38	10.56
			$S = 2$	2.41	10.91
			$S = 0$	2.37 <sup>a</sup>	10.62
	Rhombus	$D_{2h}$	$S = 2$	2.39 <sup>b</sup>	10.93
			$S = 0$	2.48	11.80
Tetrahedron	$T_d$	$S = 0$	2.48	11.80	
Trigonal pyramid	$C_{3v}$	$S = 0$	2.45, 2.42	11.79	

<sup>a</sup>With an acute angle of  $88.12^\circ$ .

<sup>b</sup>With an acute angle of  $87.28^\circ$ .

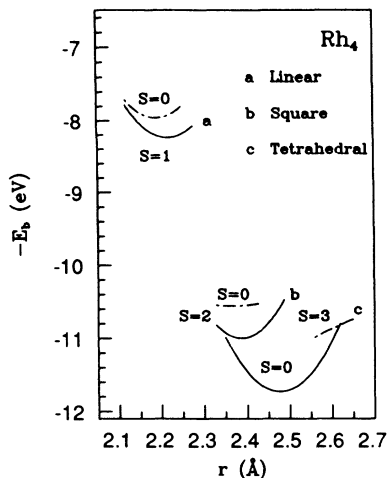


FIG. 4. Binding energy as a function of bond length for the  $\text{Rh}_4$  tetramer.

Remarkable examples are provided by the tetrahedral  $\text{Rh}_4$  cluster and the  $\text{Rh}_{10}$  cluster. For the tetrahedral  $\text{Rh}_4$  cluster, an 8% contraction causes the total magnetic moment to change from  $6\mu_B$  to  $0\mu_B$  (see Fig. 4). For the  $\text{Rh}_{10}$  cluster, only a 4% contraction changes the total moment from  $14\mu_B$  to  $6\mu_B$ . This shows the strong sensitivity of the magnetic properties of the  $\text{Rh}_N$  clusters to cluster bond length.

The size dependence of the binding energy per atom of the  $\text{Rh}_N$  clusters is displayed in Fig. 6(a). The cluster

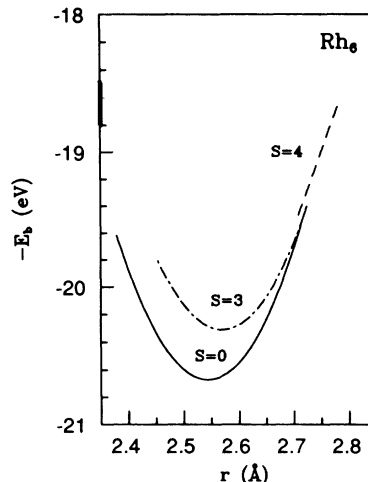


FIG. 5. Binding energy as a function of bond length for the  $\text{Rh}_6$  cluster.

binding energy per atom increases with increase of cluster size. In the region between the  $\text{Rh}_8$  and  $\text{Rh}_{19}$  clusters, the curve shows an approximately linear dependence. If we extend this linear dependence to larger clusters, we can estimate that the value of the binding energy per atom of the  $\text{Rh}_N$  cluster will reach the bulk one (5.75 eV/atom) when  $N \simeq 37$ .

The average magnetic moment per atom of the  $\text{Rh}_N$  clusters is plotted in Fig. 6(b) as a function of the number  $N$  of atoms in clusters. Here we have a complex

TABLE III. The equilibrium bond lengths and binding energies for the  $\text{Rh}_5$ - $\text{Rh}_8$ ,  $\text{Rh}_{10}$ ,  $\text{Rh}_{13}$ , and  $\text{Rh}_{19}$  clusters. Values in parentheses correspond to metastable minima.

	Symmetry	Spin	$r_e$ (Å)	$E_b$ (eV)
$\text{Rh}_5$	$D_{3h}$	$S = 3/2$	2.52	15.31
$\text{Rh}_6$	$O_h$	$S = 0$	2.54	20.74
		$(S = 3)$	2.57	20.34
$\text{Rh}_7$	$D_{5h}$	$S = 9/2$	2.58	24.03
$\text{Rh}_8$	$T_d$	$(S = 0)$	2.56	26.95
		$S = 5$	2.58	27.73
$\text{Rh}_{10}$	$D_{4d}$	$(S = 0)$	2.56	37.62
		$S = 3$	2.58	37.72
		$(S = 7)$	2.58	37.55
$\text{Rh}_{12}$	$I_h$	$(S = 0)$	2.55	46.20
		$S = 4$	2.56	46.41
		$(S = 7)$	2.56	46.01
$\text{Rh}_{13}$	$I_h$	$(S = 7/2)$	2.56 <sup>a</sup>	51.42
		$S = 15/2$	2.56 <sup>a</sup>	52.16
		$(S = 21/2)$	2.56 <sup>a</sup>	51.81
$\text{Rh}_{19}$	$D_{5h}$	$(S = 5/2)$	2.69 <sup>b</sup>	82.97
		$S = 17/2$	2.69 <sup>b</sup>	84.58

<sup>a</sup>Bond length between the central and surface atoms.

<sup>b</sup>Not optimized, taken from bulk.

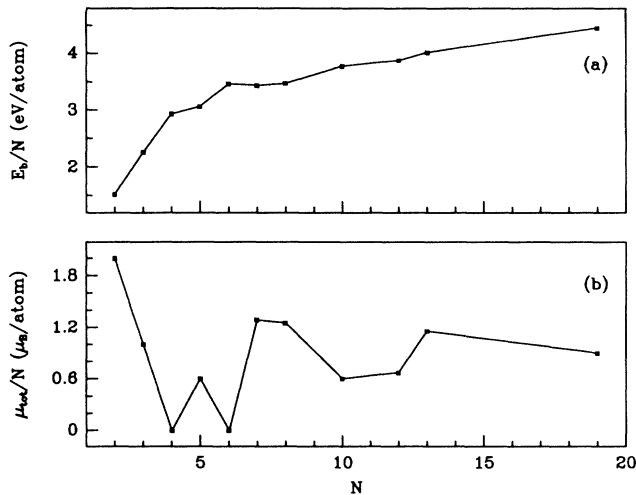


FIG. 6. Size dependence of (a) the binding energy per atom and (b) the average magnetic moment per atom of the  $Rh_N$  clusters.

size dependence of the moment, in contrast to the nearly size-independent relationship for the moment in Fe, Co, and Ni clusters.<sup>19,20,22</sup> Cox *et al.*<sup>24</sup> measured the magnetic moments per atom for  $Rh_N$  ( $N = 9-34$ ), and also found that they depend significantly on cluster size: our conclusion is consistent with their finding. As we have seen above, the average magnetic moments of the  $Rh_4$  and  $Rh_6$  clusters are zero because they have PM ground states. For the  $Rh_{10}$  and  $Rh_{12}$  clusters, the average moments per atom are  $0.60\mu_B$  and  $0.67\mu_B$ , respectively. They are in good agreement with the experimental ones<sup>24</sup> [ $(0.8 \pm 0.2)\mu_B$  and  $(0.59 \pm 0.12)\mu_B$  for  $Rh_{10}$  and  $Rh_{12}$ , respectively]. Although it is smaller than that of Reddy *et al.*,<sup>23</sup> our calculated average moment per atom for the  $Rh_{13}$  cluster ( $1.15\mu_B$ ) is still bigger than the experimental one [ $(0.48 \pm 0.13)\mu_B$ ]. For the  $Rh_{19}$  cluster, the calculated average moment per atom is  $0.89\mu_B$ , compared to  $(0.61 \pm 0.08)\mu_B$  of the experiment. We will give some possible explanations for these quantitative discrepancies between experiment and theory for  $Rh_{13}$  and  $Rh_{19}$  at the end of this section.

It is worth mentioning that we have also considered fcc-like geometries for  $Rh_{13}$  and  $Rh_{19}$ . For the fcc  $Rh_{13}$  cluster, our calculations give a  $1.46\mu_B$  average moment per atom. We obtain two magnetic solutions for the fcc  $Rh_{19}$  cluster: the average moment of the first is  $1.42\mu_B$  per atom while in the second it is  $0.58\mu_B$  per atom. The cluster binding energy for the former was calculated to be larger than that for the latter by 0.1 eV. In our calculations, the fcc-like geometries always have higher energies than the corresponding icosahedral-like geometries. At the equilibrium configurations, the icosahedral  $Rh_{13}$  cluster is more stable than the fcc  $Rh_{13}$  cluster by 1.35 eV. With the bond length at the bulk interatomic spacing, the double-icosahedral  $Rh_{19}$  cluster has bigger cluster binding energy by 4.15 eV than the fcc  $Rh_{19}$  cluster. Hence we can suggest, from the energy point of view, that the growth of Rh clusters is based on icosahedral pack-

ing. We note that icosahedral growth has been inferred for many transition-metal clusters.<sup>15</sup> For example, Parks *et al.*<sup>34</sup> suggested icosahedral growth for Ni clusters from 49 to at least 105 atoms on the basis of experimental adsorbate binding data.

Figures 7(a) and 7(b) show the densities of states (DOS) for the majority- and minority-spin electrons in the  $Rh_N$  clusters. The DOS are obtained by a Lorentzian extension of the discrete energy levels and a summation over them. The broadening width parameter is chosen to be 0.4 eV. From Fig. 7, we can see that all the DOS's

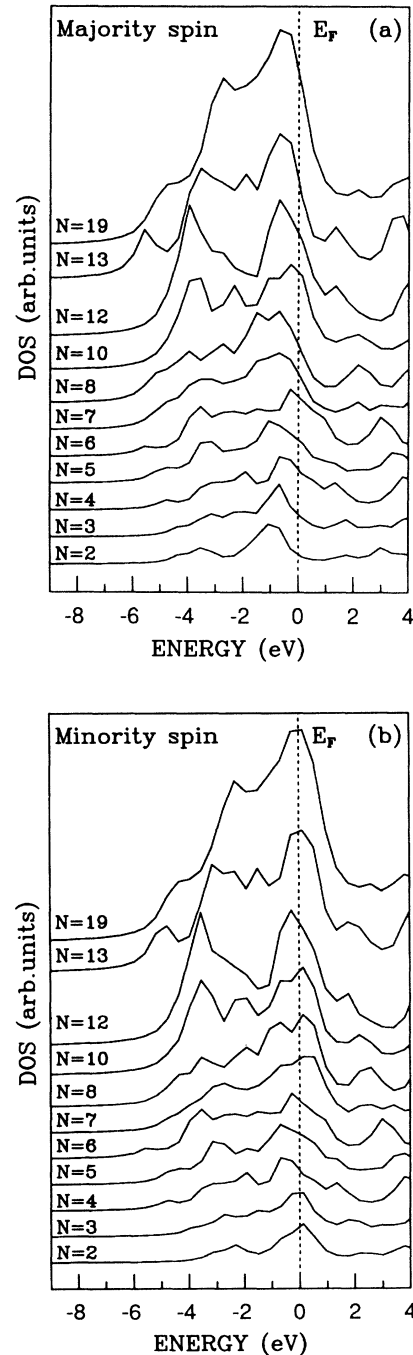


FIG. 7. DOS for the  $Rh_N$  clusters: (a) majority spin and (b) minority spin.

show a large peak near the top of the valence band, and that  $E_F$  lies in the minority peak for most clusters. This is different from the bulk where the  $E_F$  lies in a dip of the DOS.<sup>29</sup> With these figures, we can determine the exchange splitting ( $\Delta E_1$ ) and the valence band width (VBW) for each of the clusters, as listed in Table IV and plotted in Figs. 8(a) and 8(b). Comparing Fig. 8(a) with Fig. 6(b), one can find that  $\Delta E_1$  correlates in a striking way with the cluster moment: the larger the cluster moment, the larger  $\Delta E_1$ . All the VBW's of clusters are found to be smaller than the bulk value (7.0 eV). However, the variation of the VBW as a function of cluster size is somewhat complex [Fig. 8(b)]. The Rh<sub>13</sub> cluster has the largest VBW, and the VBW of Rh<sub>7</sub> is found to be smaller than those of adjacent cluster sizes. In 3d FM clusters, it has been shown<sup>12</sup> that a narrow VBW is one of the favorable conditions for enhancing the energy gain for ferromagnetism. Here we could not find any explicit correlation between the VBW and the cluster moment.

The results for the highest occupied molecular orbital (HOMO) and the lowest unoccupied molecular orbital (LUMO) of the Rh<sub>N</sub> clusters are presented in Tables IV and V and in Fig. 8(c). The gap between the HOMO and LUMO is found to be rather small for all clusters except Rh<sub>4</sub> and Rh<sub>6</sub>. For the Rh<sub>4</sub> and Rh<sub>6</sub> clusters whose ground states are PM, the gaps are 0.73 eV and 0.46 eV, respectively. From Fig. 8(c), we notice a comparatively big change in the position of the LUMO as a function of cluster size when going from Rh<sub>3</sub> to Rh<sub>4</sub> and from Rh<sub>13</sub> to Rh<sub>19</sub>. The HOMO as a function of cluster size has two local minima, at Rh<sub>6</sub> and at Rh<sub>12</sub> and Rh<sub>13</sub>, respectively. Because Rh is known to be an important catalyst, it is interesting to link the variation of the HOMO with the cluster size with the reactivity of Rh<sub>N</sub> clusters toward H<sub>2</sub>, N<sub>2</sub>, and CO molecules. Following the method of Rosen and Rantala,<sup>6</sup> we can predict that Rh<sub>5</sub>, Rh<sub>7</sub>, and Rh<sub>8</sub> clusters have substantial reactivity, while Rh<sub>6</sub>, Rh<sub>12</sub>, and Rh<sub>13</sub> show high stability toward H<sub>2</sub>, N<sub>2</sub>, and CO molecules.

For a cluster, the number of electrons in the HOMO determines its ground-state electronic configuration. From Table V, we can see that the HOMO is occupied by the minority-spin electrons for Rh<sub>2</sub>, Rh<sub>3</sub>, Rh<sub>7</sub>, Rh<sub>8</sub>, and Rh<sub>13</sub>, and by the majority-spin electrons for Rh<sub>5</sub>, Rh<sub>10</sub>, Rh<sub>12</sub>, and Rh<sub>19</sub>. This picture is very different from that

TABLE IV. The data of electronic structure for the Rh<sub>N</sub> clusters (eV).

	HOMO	LUMO	$\Delta E_1$	$\Delta E_2$	VBW
Rh <sub>2</sub>	-4.53	-4.49	1.18	0.69	4.18
Rh <sub>3</sub>	-4.23	-4.16	0.47	0.26	4.19
Rh <sub>4</sub>	-3.96	-3.23	0.00	0.73	4.40
Rh <sub>5</sub>	-3.54	-3.51	0.36	0.04	5.02
Rh <sub>6</sub>	-3.92	-3.46	0.00	0.46	5.27
Rh <sub>7</sub>	-3.59	-3.56	0.67	0.17	5.19
Rh <sub>8</sub>	-3.43	-3.43	0.69	0.11	5.40
Rh <sub>10</sub>	-3.84	-3.81	0.31	0.03	4.73
Rh <sub>12</sub>	-4.36	-4.33	0.34	0.03	4.74
Rh <sub>13</sub>	-4.33	-4.33	0.65	0.05	5.60
Rh <sub>19</sub>	-3.60	-3.53	0.48	0.07	5.21

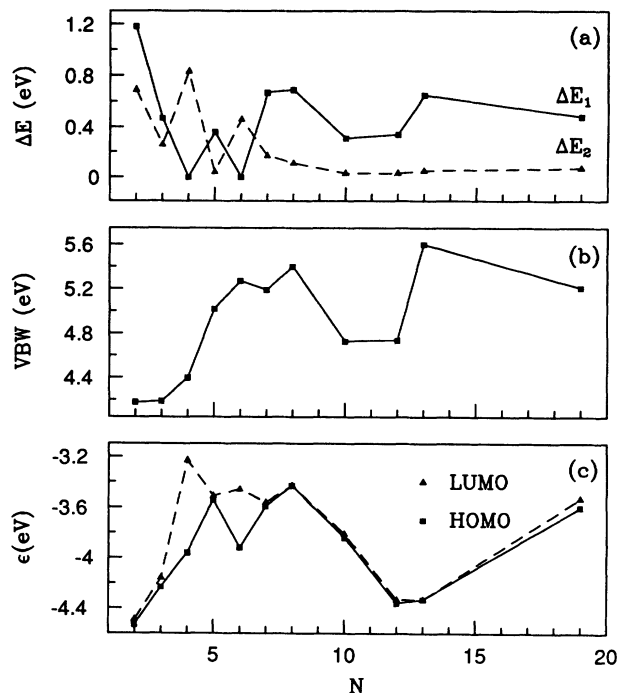


FIG. 8. Size dependence of (a)  $\Delta E_1$  and  $\Delta E_2$ , (b) the VBW, and (c) the HOMO and LUMO of the Rh<sub>N</sub> clusters.

obtained for 3d FM clusters, where the HOMO is always occupied by the minority-spin electrons.<sup>5,6,16</sup> The HOMO's of all clusters except Rh<sub>8</sub> and Rh<sub>13</sub> are fully occupied, which lead to ground states with closed electronic shells. Thus these clusters are expected to be remarkably stable. The Rh<sub>8</sub> and Rh<sub>13</sub> clusters have degenerate ground states because their HOMO's are partially occupied. According to the Jahn-Teller theorem, they tend to distort further toward lower symmetry so as to lift the degeneracy of their ground states and lower their energies. It should be emphasized, however, that the distorted cluster may also increase its energy if it changes its spin. Accordingly, it depends on a compromise between these two effects whether and to what extent the Jahn-Teller distortion may take place.

TABLE V. The ground-state electronic configurations for the Rh<sub>N</sub> clusters.

	HOMO		Electronic configuration
	Symbol	Electrons	
Rh <sub>2</sub>	$b_{3u} \downarrow$	1	closed
Rh <sub>3</sub>	$b_1 \downarrow$	1	closed
Rh <sub>4</sub>	$t_1'$	6	closed
Rh <sub>5</sub>	$a_2 \uparrow$	1	closed
Rh <sub>6</sub>	$t_{2u}$	6	closed
Rh <sub>7</sub>	$e_2'' \downarrow$	2	closed
Rh <sub>8</sub>	$t_1 \downarrow$	1	open
Rh <sub>10</sub>	$a_2 \uparrow$	1	closed
Rh <sub>12</sub>	$t_{1u} \uparrow$	3	closed
Rh <sub>13</sub>	$h_u \downarrow$	1	open
Rh <sub>19</sub>	$e_1' \uparrow$	2	closed

It is well known that the Kohn-Sham equations in the LDF scheme have a unique solution for a given system. In the LSD scheme, however, solving the equations — simultaneously optimizing the spin of the system — can yield more than one solution. These solutions correspond to local minima of the cluster energy as a function of the cluster spin. When using the LSD method, hence, we should check whether our result is the actual ground state of the system we studied. That is to say, we should know whether there are multiple magnetic solutions. When may multiple magnetic solutions exist in our LSD calculations for a system? We link the answer to an energy difference  $\Delta E_2$ , which was originally identified by us as being useful to explain the anomalous symmetry dependence of the cluster moment for  $\text{Rh}_{13}$  clusters.<sup>25</sup> For a cluster whose HOMO is partially occupied,  $\Delta E_2$  is the energy difference between the HOMO and its closest-in-energy spin-opposite molecular orbital (CSMO) which can be either occupied or unoccupied. If the HOMO is fully occupied, then  $\Delta E_2$  is either the energy difference between the HOMO and its unoccupied CSMO or between the LUMO and its occupied CSMO, depending on which one is the smaller. We suggest that when one finds  $\Delta E_2$  to be small, say, less than 0.1 eV, one should consider the possibility of multiple solutions in the LSD calculation.

The values of  $\Delta E_2$  for the  $\text{Rh}_N$  clusters are listed in Table IV and plotted in Fig. 8(a). From the table and figure, we can see that the  $\text{Rh}_2$ – $\text{Rh}_4$ , and  $\text{Rh}_6$ – $\text{Rh}_8$  clusters have comparatively large  $\Delta E_2$ , while the value of  $\Delta E_2$  for the  $\text{Rh}_5$  and  $\text{Rh}_{10}$ – $\text{Rh}_{19}$  clusters is smaller than 0.1 eV. Actually, one can see from Table III that, at their equilibrium configurations, the  $\text{Rh}_2$ – $\text{Rh}_4$ , and  $\text{Rh}_6$ – $\text{Rh}_8$  clusters have only one self-consistent magnetic solution, and the  $\text{Rh}_{10}$ – $\text{Rh}_{19}$  clusters have two or three self-consistent magnetic solutions. These results are in accordance with our  $\Delta E_2$  criterion for the existence of multiple magnetic solutions. For  $\text{Rh}_5$ , the small  $\Delta E_2$  suggests it might have multiple solutions, while one can see only one self-consistent solution with  $S = 3/2$  for it in Table III. We can explain this discrepancy as follows. For  $\text{Rh}_5$ , the energy difference between the HOMO and its unoccupied CSMO is 0.04 eV (i.e.,  $\Delta E_2$ ), while the energy difference between the LUMO and its occupied CSMO is 0.44 eV. Since the HOMO is occupied by a majority-spin electron (Table V), another self-consistent magnetic solution one can expect for the cluster in addition to the solution with  $S = 3/2$  is the one with  $S = 1/2$ . In our calculations, where levels are occupied according to Fermi-Dirac statistics at 0 K, the cluster spin  $S$  is only permitted to change by an integer number. Hence the energy, seen as a function of  $S$ , is only defined for values of its argument differing by integers and thus cannot have two local minima corresponding to adjacent values of  $S$ .

The results for Mulliken orbital and spin populations evaluated for the  $\text{Rh}_N$  clusters are given in Table VI and Fig. 9. With reference to the atomic configuration  $4d^8 5s^1 5p^0$ , one can easily see how the electron of the  $5s$  is redistributed to the  $4d$  and  $5p$  with the increase of cluster size. Spin populations show some common features with the magnetism for Rh clusters. For example, all clus-

TABLE VI. Mulliken orbital and spin populations for the  $\text{Rh}_N$  clusters.  $a$ ,  $b$ ,  $c$ , and  $d$  are the types of inequivalent atoms within the cluster point group, and the number of atoms of each inequivalent type is given in parentheses.

		Charge			Net spin			Total
		4d	5s	5p	4d	5s	5p	
$\text{Rh}_2$		8.18	0.75	0.06	1.74	0.23	0.02	2.00
$\text{Rh}_3$	$a(1)$	8.16	0.66	0.12	1.00	0.00	0.00	1.00
	$b(2)$	8.18	0.72	0.13	0.99	0.00	0.01	1.00
$\text{Rh}_4$		8.24	0.58	0.18	0.00	0.00	0.00	0.00
$\text{Rh}_5$	$a(2)$	8.27	0.56	0.13	0.52	-0.04	0.04	0.52
	$b(3)$	8.21	0.52	0.28	0.67	-0.01	0.01	0.67
$\text{Rh}_6$		8.25	0.48	0.27	0.00	0.00	0.00	0.00
$\text{Rh}_7$	$a(2)$	8.12	0.50	0.40	1.37	-0.02	0.02	1.37
	$b(5)$	8.25	0.53	0.23	1.29	-0.05	0.02	1.26
$\text{Rh}_8$	$a(4)$	8.10	0.53	0.49	1.36	-0.03	-0.05	1.28
	$b(4)$	8.29	0.51	0.08	1.26	-0.07	0.04	1.23
$\text{Rh}_{10}$	$a(2)$	8.22	0.61	0.15	0.65	0.08	0.03	0.76
	$b(8)$	8.19	0.51	0.32	0.54	0.00	0.01	0.55
$\text{Rh}_{12}$		8.15	0.55	0.30	0.52	0.11	0.04	0.67
$\text{Rh}_{13}$	$a(1)$	7.92	0.40	0.66	1.32	0.00	-0.20	1.12
	$b(12)$	8.14	0.53	0.33	0.99	0.10	0.07	1.16
$\text{Rh}_{19}$	$a(2)$	7.90	0.46	0.56	0.98	0.00	-0.05	0.93
	$b(2)$	8.16	0.46	0.28	0.81	-0.03	0.03	0.81
	$c(5)$	8.10	0.49	0.52	0.71	0.04	0.00	0.75
	$d(10)$	8.17	0.52	0.29	0.90	0.03	0.05	0.98

ters with magnetic ground states have FM interactions, the cluster moment mainly comes from the  $4d$  local moment, and the local moments of the  $5s$  and  $5p$  often align antiferromagnetically with that of the  $4d$ .

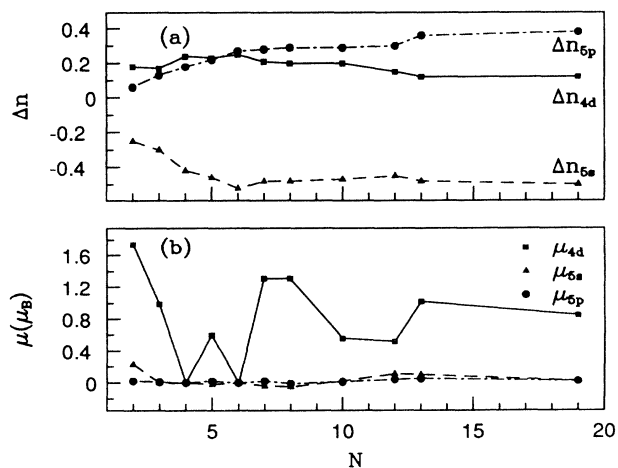


FIG. 9. Size dependence of (a) Mulliken orbital populations, where  $\Delta n_{4d} = n_{4d} - 8$ ,  $\Delta n_{5s} = n_{5s} - 1$ , and  $\Delta n_{5p} = n_{5p}$ , and (b) Mulliken spin populations of the  $\text{Rh}_N$  clusters.

Finally, let us discuss the origins of the quantitative discrepancies of the magnetic moment between experiment and theory for Rh<sub>13</sub> and Rh<sub>19</sub>. For Rh<sub>13</sub>, our explanation is that the real cluster geometry is not a perfect icosahedron, but it is instead a distorted one, and undergoing distortion decreases the total magnetic moment of the cluster. Such an expectation is reasonable because we have shown that the perfect icosahedral Rh<sub>13</sub> has a tendency to undergo Jahn-Teller distortion, and that there is already a low-spin magnetic solution ( $S = 7/2$ ) for the perfect icosahedral Rh<sub>13</sub>, though it has not the lowest energy of this geometry. The fact that we have not optimized the bond lengths of the Rh<sub>19</sub> cluster could possibly be reasoned to be the origin of the discrepancy for Rh<sub>19</sub>. Moreover, the fact that the low-spin magnetic solution ( $S = 5/2$ ) for Rh<sub>19</sub> is AFM would make a direct comparison between theory and experiment impossible, if this solution became the ground-state solution after optimization. The experiment only measures the time-averaged magnetic moment of a cluster and not the internal moment itself.<sup>24</sup> The true internal moment is deduced by applying the superparamagnetism model.<sup>10</sup> Whether the superparamagnetism model without some corrections can be applied to AFM clusters is still questioned.

#### IV. SUMMARY

In this paper, we have reported a comprehensive study of the structural, electronic, and magnetic properties of small Rh clusters, using the first-principles DV-LSD method. The results we have obtained can be summarized as follows.

(1) The ground-state structures of Rh<sub>2</sub>, Rh<sub>3</sub>, and Rh<sub>4</sub> are obtained. The results show that the systems prefer higher-dimensional geometries with longer bond lengths and more nearest-neighbor bonds.

(2) The bond lengths in the chosen geometry for the Rh<sub>5</sub>-Rh<sub>8</sub>, Rh<sub>10</sub>, Rh<sub>12</sub>, and Rh<sub>13</sub> clusters are optimized. Compared with the bulk interatomic spacing, bond-length contractions are found in all clusters and have

dramatically changed the magnetic properties of some clusters.

(3) A complex size dependence of the magnetic properties of the Rh<sub>N</sub> clusters is found, consistent with a recent experiment. The average magnetic moment per atom of the Rh<sub>N</sub> clusters varies from  $0\mu_B$  to  $2\mu_B$ . The clusters with magnetic ground states have FM interactions, while the local moments of the  $5s$  and  $5p$  often align antiferromagnetically with that of the  $4d$ . The calculated magnetic moments of the Rh<sub>10</sub> and Rh<sub>12</sub> clusters are in good agreement with the experimental ones. Possible origins are proposed to explain the quantitative discrepancies between experiment and theory for the magnetic moment for Rh<sub>13</sub> and Rh<sub>19</sub> clusters.

(4) Icosahedral growth is suggested for Rh clusters based on studies of the binding energy for the icosahedral-like and fcc-like Rh<sub>13</sub> and Rh<sub>19</sub> clusters.

(5) The electronic properties of the Rh<sub>N</sub> clusters are calculated. The DOS,  $\Delta E_1$ , and VBW are presented and discussed with the cluster size and magnetic moment.

(6) The HOMO and LUMO are extensively analyzed for the Rh<sub>N</sub> clusters. The results obtained reveal that (a) all clusters except Rh<sub>4</sub> and Rh<sub>6</sub> have small energy gaps, (b) the Rh<sub>5</sub>, Rh<sub>7</sub>, and Rh<sub>8</sub> clusters have substantial reactivity, while Rh<sub>6</sub>, Rh<sub>12</sub>, and Rh<sub>13</sub> show high stability toward H<sub>2</sub>, N<sub>2</sub>, and CO molecules, and (c) the Rh<sub>8</sub> and Rh<sub>13</sub> clusters have open electronic shells and are expected to distort further according to the Jahn-Teller theorem.

(7) The energy parameter  $\Delta E_2$  is introduced and tested as the criterion for the existence of multiple magnetic solutions in LSD calculations.

#### ACKNOWLEDGMENTS

This work was supported by the Ministero della Pubblica Istruzione through INFM and by CEE through Human Capital and Mobility Network Contract No. ERBCHRX-CT920075. One of us (Y.J.) gratefully acknowledges the hospitality of GNSM in Padova, the encouragement from GCMT in Hefei, and the financial support of CNR (Italy) and CAS (China).

\* Mailing address.

<sup>1</sup> For a review, see *Proceedings of the Sixth International Meeting on Small Particles and Inorganic Clusters*, Chicago, 1992 [Z. Phys. D **26** (1993)].

<sup>2</sup> E.P. Wohlfarth, Phys. Status Solidi A **91**, 339 (1985).

<sup>3</sup> M.R. Zapkin, D.M. Cox, R.O. Brickman, and A.J. Kaldor, J. Phys. Chem. **93**, 6823 (1989).

<sup>4</sup> D.R. Salahub and R.P. Messmer, Surf. Sci. **106**, 415 (1981).

<sup>5</sup> K. Lee, J. Callaway, and S. Dhar, Phys. Rev. B **30**, 1724 (1985).

<sup>6</sup> A. Rosen and T.T. Rantala, Z. Phys. D **3**, 205 (1986).

<sup>7</sup> G.M. Pastor, J. Dorantes-Davila, and K.H. Benneman, Phys. Rev. B **40**, 7642 (1989).

<sup>8</sup> N. Fujima and T. Yamaguchi, J. Phys. Soc. Jpn. **58**, 3290 (1989).

<sup>9</sup> B.I. Dunlap, Phys. Rev. A **41**, 5691 (1990).

<sup>10</sup> S.N. Khanna and S. Linderoth, Phys. Rev. Lett. **67**, 742 (1991).

<sup>11</sup> F. Liu, S.N. Khanna, and P. Jena, Phys. Rev. B **43**, 8179 (1991).

<sup>12</sup> J.L. Chen, C.S. Wang, K.A. Jackson, and M.R. Pederson, Phys. Rev. B **44**, 6558 (1991).

<sup>13</sup> Z.Q. Li and B.L. Gu, Phys. Rev. B **47**, 13 611 (1993).

<sup>14</sup> O.B. Christensen and M.L. Cohen, Phys. Rev. B **47**, 13 643 (1993).

<sup>15</sup> C. Rey, L.J. Gallego, J. Garcia-Rodeja, J.A. Alonso, and M.P. Iniguez, Phys. Rev. B **48**, 8253 (1993).

<sup>16</sup> Yang Jinlong, Xiao Chuanyun, Xia Shangda, and Wang Kelin, Phys. Rev. B **48**, 12 155 (1993).

<sup>17</sup> K. Lee and J. Callaway, Phys. Rev. B **48**, 15 358 (1993).

<sup>18</sup> D.M. Cox, D.J. Trevor, R.L. Whetten, E.A. Rohlfling, and A. Kaldor, J. Chem. Phys. **84**, 4651 (1986).

<sup>19</sup> W.A. deHeer, P. Milani, and A. Chatelain, Phys. Rev. Lett. **65**, 488 (1990).

<sup>20</sup> J.P. Bucher, D.C. Douglass, and L.A. Bloomfield, Phys. Rev. Lett. **66**, 3052 (1991).

- <sup>21</sup> D.C. Douglass, J.P. Bucher, and L.A. Bloomfield, *Phys. Rev. B* **45**, 6341 (1992).
- <sup>22</sup> J.G. Louderback, A.J. Cox, L.J. Lising, D.C. Douglass, and L.A. Bloomfield, *Z. Phys. D* **26**, 301 (1993).
- <sup>23</sup> B.V. Reddy, S.N. Khanna, and B.I. Dunlap, *Phys. Rev. Lett.* **70**, 3323 (1993).
- <sup>24</sup> A.J. Cox, J.G. Louderback, and L.A. Bloomfield, *Phys. Rev. Lett.* **71**, 923 (1993); *Phys. Rev. B* **49**, 12 295 (1994).
- <sup>25</sup> Yang Jinlong, F. Toigo, Wang Kelin, and Zhang Manhong, *Phys. Rev. B* **50**, 7173 (1994).
- <sup>26</sup> B. Delley and D.E. Ellis, *J. Chem. Phys.* **76**, 1949 (1982).
- <sup>27</sup> B. Delley, D.E. Ellis, A.J. Freeman, E.J. Baerends, and D. Post, *Phys. Rev. B* **27**, 2132 (1983).
- <sup>28</sup> U. von Barth and L. Hedin, *J. Phys. C* **5**, 1629 (1972).
- <sup>29</sup> V.L. Moruzzi, J.F. Janak, and A.R. Williams, *Calculated Electronic Properties of Metals* (Pergamon, New York, 1978).
- <sup>30</sup> J.P. Perdew and A. Zunger, *Phys. Rev. B* **23**, 5048 (1981).
- <sup>31</sup> K.A. Gingerich and D.L. Cocke, *J. Chem. Soc. Commun.* **1**, 536 (1972).
- <sup>32</sup> I. Shim, *Mat.-Fys. Meddr. Danske Vidensk. Selsk* **41**, 147 (1985).
- <sup>33</sup> D.R. Salahub, *Adv. Chem. Phys.* **65**, 447 (1987).
- <sup>34</sup> E.K. Parks, B.J. Winter, T.D. Klots, and S.J. Riley, *J. Chem. Phys.* **94**, 1882 (1991).